

Formation of η -mesic nuclei by (π, N) reaction and $N^*(1535)$ in medium

Hideko Nagahiro,¹ Daisuke Jido,² and Satoru Hirenzaki³

¹Research Center for Nuclear Physics(RCNP), Osaka University, Ibaraki, Osaka, 567-0047, Japan

²Yukawa Institute for Theoretical Physics, Kyoto University, Kyoto 606-8502, Japan

³Department of Physics, Nara Women's University, Nara, 630-8506, Japan

We calculate formation spectra of η -nucleus systems in (π, N) reactions with nuclear targets, which can be performed at existing and/or forthcoming facilities, including J-PARC, in order to investigate η -nucleus interactions. Based on the $N^*(1535)$ dominance in the ηN system, η -mesic nuclei are suitable systems for study of in-medium properties of the $N^*(1535)$ baryon resonance, such as reduction of the mass difference of N and N^* in nuclear medium, which affects level structure of the η and N^* -hole modes. We find that clear information on the in-medium N^* - and η -nucleus interactions can be obtained through the formation spectra of the η -mesic nuclei. We also discuss the experimental feasibilities by showing several spectra of (π, N) reactions calculated with possible experimental settings. Coincident measurements of πN pairs from the N^* decays in nuclei help us to reduce backgrounds.

PACS numbers: 21.85.+d, 21.65.Jk, 12.39.Fe, 14.20.Gk, 14.40.Aq, 25.80.Hp

I. INTRODUCTION

The study of meson-nucleus bound systems is one of the important subjects in nuclear physics. The detailed investigations of structure of bound states provide us quantitative information on hadron-nucleus interactions. So far, the structure of atomic states of pion, kaon, and \bar{p} have been successfully observed and investigated comprehensively both in theoretical and experimental points of view [1]. One of the remarkable developments in experimental aspects is the establishment of $(d, {}^3\text{He})$ spectroscopy for the formation of deeply bound pionic atoms with recoil free kinematics [2, 3, 4, 5]. It opens new possibilities of the formation of other hadron-nucleus bound systems [6, 7, 8, 9, 10].

The bound states of the η meson in nuclei were predicted first by Haider and Liu [11]. After that many works were devoted to studies of the structure of the bound states, the formation reactions of η -mesic nuclei and in-medium properties of the η meson [6, 7, 9, 10, 12, 13, 14, 15, 16, 17, 18, 19, 20, 21]. Especially, the η meson in nuclear medium has been recently investigated in the aspect of chiral symmetry [6, 7, 9, 10, 15, 16, 17, 18, 20]. The η -nucleus systems are purely governed by strong interactions in contrast to the atomic states of mesons with negative charge. Thus, the η mesons in the bound states are largely overlapped with nuclei. In such compact systems, large medium effects on the mesons inside nuclei are expected, and, at the same time, wide natural widths of the bound states due to absorptions of the mesons into the nucleus are inevitable, as seen deeply bound kaonic nuclei [22].

The first experimental search of the η bound states in nuclei [23] was performed in (π^+, p) reactions with several nuclear targets in finite momentum transfer to aim to observe narrow states as predicted in Ref. [11], and the result turned out to be negative. Some hints of the η bound states were also observed as enhancement at the subthreshold of the η meson production in

$d(p, {}^3\text{He})\eta$ [24] and ${}^{18}\text{O}(\pi^+, \pi^-){}^{18}\text{Ne}$ [25] reactions. Observation of a η meson bound state in ${}^3\text{He}$ was reported in photoproduction reactions [26], though interpretation of these observations are still controversial [27]. It was suggested in Ref. [28] that coincident observation of πN pairs from $N^*(1535)$ helps to identify the formation of η meson bound states. Other experiments have been also proposed [29, 30, 31, 32].

The study of the hadron properties in nuclear medium is largely related to the fate of chiral symmetry in finite density. It is expected that partial restoration of chiral symmetry in nuclear medium takes place as reduction of the quark condensates [33, 34] and provides effective change of the hadron properties. For the context of the study of the η meson in nuclear medium, the $N^*(1535)$ resonance, which can be a candidate of the chiral partner of the nucleon becoming degenerate in the chiral restoration limit [35, 36, 37], plays an important role in the η -mesic nuclei due to the strong coupling of the η -nucleon system to the $N^*(1535)$ resonance. In our previous works [9, 10, 18], it was found that the η optical potential in nuclei is strongly sensitive to the in-medium mass gap of N and $N^*(1535)$ and that, as a consequence, the formation spectra of the η -mesic nuclei is also sensitive to the in-medium properties of the $N^*(1535)$.

The sensitivity of the η -nucleus optical potential to the N - N^* mass gap stems from possible level crossing between N^* -hole and η modes in nuclear medium as suggested in Ref. [20]. The level difference between the N^* -hole and η modes without medium effects is only 50 MeV, which is 10% of the N - N^* mass gap and small enough in energy scale of hadronic interactions. We found that the level crossing caused by the reduction of the mass gap provides deep η bound states and significant enhancement of the formation spectra of the η -mesic nuclei in the quasi-free η production energies. This will be a clue to deduce the in-medium N^* properties for the η -mesic nuclei.

In this paper, we revisit the (π, N) reaction with the

recoil free kinematics for the formation of η -mesic nuclei in order to get clearer information on the level structure of the η and N^* -hole modes and in-medium properties of $N^*(1535)$ in the viewpoint of the chiral symmetry for baryons. We will find that the appropriate kinetic energy of the injecting pion in this reaction can be attained by the Japan Proton Accelerator Research Complex (J-PARC) facility. We will also compare our calculation with the old experiments of the (π^+, p) reaction with finite momentum transfer [23], in which the expected peak structures predicted in Ref. [11] were not found. In this paper, we discuss more appropriate experimental conditions than the old experiments and also propose the coincidence observation to reduce large background, which would be one of the reasons why the experiment [23] could not see the expected peak structure.

This paper is organized as follows. In Sec. II, we discuss the properties of the η spectral functions in the nuclear matter. In Sec. III, we introduce the η -nucleus optical potentials with a finite size nucleus and discuss their features. The formation spectra of η -mesic nuclei will be shown in Sec. IV, and the physical meaning of the formation spectra will be discussed. In Sec. V we will discuss the experimental feasibilities, and finally, we will devote Sec. VI to summary of this paper.

II. LEVEL CROSSING OF THE η MESON AND N^* -HOLE MODES

In this section, we briefly review the interesting feature of the η meson in nuclear medium pointed out in Ref. [20]. Reduction of the mass gap between N and N^* causes level crossing of the η and N^* -hole modes, and consequently the η spectral function in nuclear medium has significant properties.

The in-medium η propagator is given by,

$$D_\eta(\omega, k; \rho)^{-1} = \omega^2 - k^2 - m_\eta^2 - \Pi_\eta(\omega, k; \rho), \quad (1)$$

where ω and k denote the energy and momentum of the η meson, m_η is its mass, and Π_η denotes the η self-energy in the nuclear medium. Because of the strong coupling of the ηN system to the $N^*(1535)$ resonance, the η self-energy Π_η can be evaluated by the N^* dominance. Considering one N^* -nucleon-hole excitation, we obtain the η self-energy in small η momentum [9, 20] as

$$\Pi_\eta(\omega, k; \rho) = \frac{g_\eta^2 \rho}{\omega + m_N^*(\rho) - m_{N^*}^*(\rho) + i\Gamma_{N^*}(\omega, \rho)/2} + (\text{cross term}). \quad (2)$$

Here, g_η is the coupling constant of the s -wave ηNN^* vertex and can be determined to $g_\eta \simeq 2.0$ to reproduce the in-vacuum partial width $\Gamma_{N^* \rightarrow \eta N} \simeq 75$ MeV [38] at tree level. $m_N^*(\rho)$ and $m_{N^*}^*(\rho)$ are effective masses of N and N^* in the nuclear medium with density ρ , respectively.

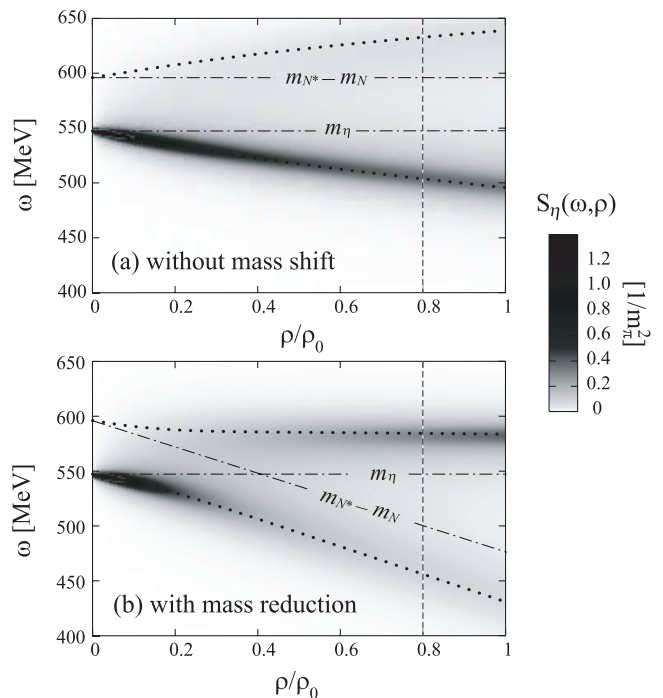


FIG. 1: Contour maps of the η meson spectral density in nuclear matter in Eq. (3) as functions of the baryon density and energy assuming (a) the N and N^* masses not to change in medium and (b) 20% mass gap reduction of N and N^* at normal nuclear density ρ_0 . In this figure, the N^* width in medium is fixed to be constant $\Gamma_{N^*} = 75$ MeV for simplicity. The dotted lines indicate the real parts of the solutions of $D_\eta(\omega, k=0; \rho)^{-1} = 0$ in Eq. (1).

The η propagator (1) with the self-energy (2) has two poles with a positive real part in the complex energy plane in each density. These poles describe the η meson and N^* -hole modes in nuclear medium [15, 16, 20]. Corresponding to these poles, the η spectral density S_η given

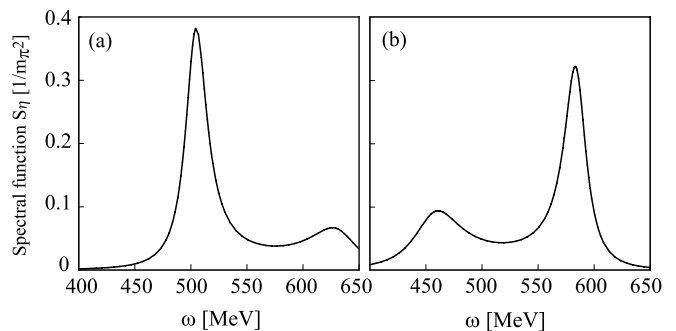


FIG. 2: Spectral functions of the η meson as functions of the η energy at $\rho/\rho_0 = 0.8$ (indicated by the vertical dashed lines in Fig. 1) (a) without mass shift and (b) with 20% mass gap reduction of N^* and N at normal nuclear density.

by

$$S_\eta(\omega, \rho) = -\frac{1}{\pi} \text{Im}(D_\eta(\omega, k=0; \rho)) \quad (3)$$

has two peaks in a function of real energy at a certain density.

We show the contour maps of the η spectral density as functions of baryon density and η energy in Fig. 1, where the real parts of the pole positions are indicated by dotted lines. Figure 1(a) shows the strength of two branches in the case that the effective masses of N and N^* do not change in medium. In this case, two branches slightly come away from each other for higher ρ as a result of level repulsion, and the strength of the lower mode is always larger than the upper mode as also shown explicitly in Fig. 2(a). The similar behavior of the η spectral function based on the chiral unitary approach were also reported in Refs. [15, 16], where the reduction of the mass gap between N and N^* is very small. In contrast, in the case that the mass gap becomes smaller in nuclear medium, the behavior of the η spectral density significantly changes. Suppose that the mass gap of N and N^* linearly decreases by 20% at ρ_0 , the level crossing between two branches takes place around $\rho \sim 0.4\rho_0$ as shown in Fig. 1(b). As a consequence, the strength of the upper mode becomes stronger due to the level mixing, and the lower mode shifts downwards considerably as the density increases.

A possible source of the mass gap reduction is the partial restoration of chiral symmetry in nuclear medium. If $N^*(1535)$ is a chiral partner of nucleon, the N and N^* mass difference should decrease as chiral symmetry is being restored. For the later discussion, we use the following parameterization of the mass gap reduction based on the chiral doublet model [36, 37]:

$$m_{N^*}^*(\rho) - m_N^*(\rho) = \left(1 - C \frac{\rho}{\rho_0}\right) (m_{N^*} - m_N), \quad (4)$$

where m_N and m_{N^*} are the N and N^* masses in free space, respectively. Here the parameter C represents the strength of the chiral restoration at the normal nucleon saturation density ρ_0 , and its empirical value lies from 0.1 to 0.3 [39]. Figures 1(b) and 2(b) correspond to the case with $C = 0.2$ [40] in the chiral doublet model.

These characteristic phenomena caused by the level crossing can be a signal of the reduction of the N and N^* mass gap, which supports the partial restoration of the chiral symmetry in nuclear medium. In next section, we introduce the η -nucleus optical potentials for the study in finite size systems.

III. η -NUCLEUS OPTICAL POTENTIALS

As discussed in the previous section, with the sufficient reduction of the N - N^* mass gap, the level crossing between the η and N^* -hole modes takes place at certain density in nuclear medium. As a consequence of the

level crossing, the in-medium η self-energy has strong energy dependence. In addition, the mass gap reduction as density increases gives also strong density dependence on the η self-energy as pointed out in Ref. [9]. In this section we see that the η optical potential in nuclei also has these features, and we briefly explain the models for the in-medium N^* which we use in the calculation of the formation spectra of the η -mesic nuclei. The details are described in Refs. [9, 10, 18, 20].

For the in-medium properties of N^* , we use two kinds of the chiral models, which are based on distinct physical pictures of N^* . One is the chiral doublet model [35, 36, 37], in which N^* is regarded as the chiral partner of the nucleon. The other is the chiral unitary model, in which N^* is dynamically generated resonance in the coupled channel meson-baryon scattering [16, 17].

In the first approach, the N^* is introduced as a particle with a large width and appears in an effective Lagrangian together with the nucleon field in linear realization of chiral symmetry. The η -nucleus optical potential can be obtained from the η self-energy (2):

$$\begin{aligned} V_\eta(\omega, r) &\equiv \frac{\Pi_\eta(\omega, k=0; \rho(r))}{2\mu} \\ &= \frac{g_\eta^2}{2\mu \omega + m_N^*(\rho(r)) - m_{N^*}^*(\rho(r)) + i\Gamma_{N^*}(\omega, \rho(r))/2} \\ &\quad + (\text{cross term}). \end{aligned} \quad (5)$$

Here we use the local density approximation and heavy baryon limit [14], and the density-dependent mass difference $m_N^* - m_{N^*}^*$ are given in Eq. (4). We can ignore the momentum k of the η meson because we consider almost recoilless production of the η meson in the following sections. We use an empirical density distribution of nucleons in Woods-Saxon form:

$$\rho(r) = \frac{\rho_0}{1 + \exp\left(\frac{r-R}{a}\right)}, \quad (6)$$

with $R = 1.18A^{1/3} - 0.48$ fm, $a = 0.5$ fm and the nuclear mass number A .

The optical potential (5) is sensitive to the mass difference of N and N^* in nuclei. Especially, the sign of the real part of the η optical potential changes when the mass gap of N^* and N becomes smaller than the η energy ω [9, 10, 18]. This means that the attractive η -nucleus interaction at low densities can turn to be repulsive depending on the values of the mass gap and the η energy. This feature can be seen in Fig. 3(a), where we plot the η -nucleus optical potentials as functions of radial coordinate r at η energies. For instance, at the η threshold $\omega = m_\eta$, the optical potential has a repulsive core inside the nucleus and an attractive pocket on the surface. Furthermore, this mass reduction yields also the strong energy dependence of the η -nucleus optical potential as shown in Fig. 3(a). At $\omega \simeq m_\eta - 100$ MeV, the real part of the optical potential is about 140 MeV attractive while that of the η threshold $\omega = m_\eta$ is 55 MeV repulsive at $r = 0$.

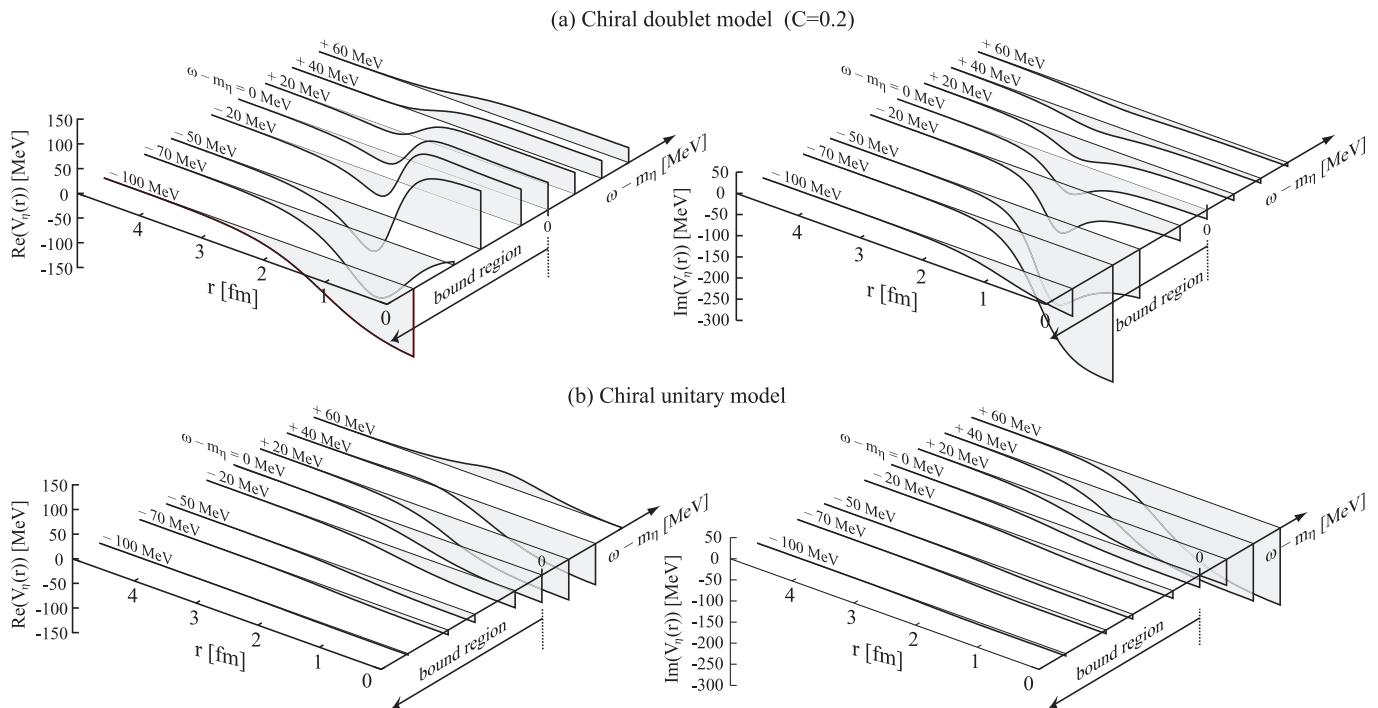


FIG. 3: The η -nucleus optical potentials with (a) the chiral doublet model ($C = 0.2$) and (b) the chiral unitary model as functions of the radial coordinate r for η energies $\omega - m_\eta = -100, -70, -50, -20, 0, +20, +40, +60$ MeV. Left and right figures show the real and imaginary parts of the optical potentials V_η , respectively.

In order to discuss the experimental feasibilities of mesic-nuclei formations, it is very important to estimate the imaginary parts of the optical potentials. As for the N^* width in the medium which is the source of the imaginary potentials in the present model, we consider the two dominant decay channels of N^* as $N^* \rightarrow N\pi$ and $NN^* \rightarrow NN\pi$ [9, 10]. The detailed evaluation is given in Ref. [20].

In the chiral doublet model, there are two possible models concerning the assignment of the axial charge: the naive and mirror assignments [36, 37]. In this paper, we show only the results with the naive assignment of the chiral doublet model. The difference between two assignments in this study appears only in the estimation of the N^* width in nuclear medium, because the representation of the mass gap $m_N^*(\rho) - m_{N^*}^*(\rho)$ is same in the both assignments. We have already checked the calculated spectra with the mirror assignment are almost same as that of the naive assignment [10, 18].

In the second approach to description of N^* , which is the chiral unitary model, the optical potential has quite different features from the previous case. In this model, it was found that N^* has a dominant component of the $K\Sigma$ channel [41, 42, 43]. Since the Σ hyperon is free from the Pauli blocking in the nuclear medium, only tiny change of the mass gap is expected in the nuclear medium [15, 16]. Therefore, the η optical potential is attractive in the bound energy region, $\omega \leq m_\eta$, as shown in Fig. 3(b), and has weaker energy dependence compared with that

of the chiral doublet model. We evaluate the η optical potential in the chiral unitary model using the η self-energy obtained in Ref. [16]. The binding energies and widths of the η bound states obtained with the chiral unitary model are reported in Ref. [17].

In recent works [44], it was pointed out that the $N^*(1535)$ obtained in the chiral unitary model could have some components other than the state generated dynamically by meson-baryon scattering, such as genuine quark states, and that these components could be sources of the chiral partner of the $N^*(1535)$. The would-be quark components are implemented in the subtraction constants, which are model parameters in the chiral unitary approach. In the present model for $N^*(1535)$ in nuclear medium, the subtraction constants were assumed to be fixed. This means that the genuine quark components are independent on medium modifications in this model. This could be the origin of the different predictions on the in-medium $N^*(1535)$ mass.

IV. (π, N) REACTION FOR THE FORMATION OF THE η -NUCLEUS SYSTEM

A. Formulation

In the beginning of this section, we give the formulation to calculate the formation spectra of the η -mesic nuclei by (π^+, p) reaction. We use the same formulation used

in Ref. [18], in which the (γ, p) reaction was discussed for the η -mesic nuclei.

To evaluate the formation cross section, we use the Green's function method [45]. In this method, the reaction cross section is assumed to be separated into the nuclear response function $R(E)$ and the elementary cross section of the $\pi^+ n \rightarrow p\eta$ process with the impulse approximation:

$$\left(\frac{d^2\sigma}{d\Omega dE} \right)_{A(\pi^+, p)(A-1)\eta} = \left(\frac{d\sigma}{d\Omega} \right)_{n(\pi^+, p)\eta}^{lab} \times R(E), \quad (7)$$

where the nuclear response function $R(E)$ is given in terms of the in-medium Green's function $G(E)$ as

$$R(E) = -\frac{1}{\pi} \text{Im} \sum_f \mathcal{T}_f^\dagger G(E) \mathcal{T}_f \quad (8)$$

where the summation is taken inclusively over all possible final states. The amplitude \mathcal{T}_f describes the transition of the incident π to a neutron hole and the outgoing proton:

$$\mathcal{T}_f(\mathbf{r}) = \chi_p^*(\mathbf{r}) \xi_{1/2, m_s}^* \left[Y_{l_\eta}^*(\hat{r}) \otimes \psi_{j_n}(\mathbf{r}) \right]_{JM} \chi_\pi(\mathbf{r}) \quad (9)$$

with the neutron hole wavefunction ψ_{j_n} , the distorted waves of π and the ejected proton χ_π and χ_p , the η angular wavefunction $Y_{l_\eta}(\hat{r})$ and the spin wavefunction $\xi_{1/2, m_s}$ of the ejected proton. For the neutron hole, we use the harmonic oscillator wavefunction. The Green's function $G(E)$ contains the η -nucleus optical potential in the Hamiltonian as

$$G(E; \mathbf{r}, \mathbf{r}') = \langle n^{-1} | \phi_\eta(\mathbf{r}) \frac{1}{E - H_\eta + i\epsilon} \phi_\eta^\dagger(\mathbf{r}') | n^{-1} \rangle \quad (10)$$

where ϕ_η^\dagger is the η creation operator and $|n^{-1}\rangle$ is the neutron hole state.

As for the evaluation of the distortion effect of the (π^+, p) reaction, we use the eikonal approximation for the description of the distorted waves of the incoming pion χ_π and of the outgoing proton χ_p as,

$$\chi_p^*(\mathbf{r}) \chi_\pi(\mathbf{r}) = \exp[i\mathbf{q} \cdot \mathbf{r}] F(\mathbf{r}) \quad (11)$$

with the momentum transfer between pion and proton $\mathbf{q} = \mathbf{p}_\pi - \mathbf{p}_p$. The distortion factor $F(\mathbf{r})$ is defined as in Eqs. (17) and (18) in Ref. [18], using pion-nucleon and proton-nucleon total cross sections [38] to take into account the distortion effects to projectile(pion) and ejectile(proton).

The calculation of the formation spectra is done separately in subcomponents of the η -mesic nuclei label by $(n\ell_j)_n^{-1} \otimes \ell_\eta$, which means a configuration of a neutron-hole in the ℓ orbit with the total spin j and the principle quantum number n in the daughter nucleus and an η meson in the ℓ_η orbit. The total formation spectra are obtained by summing up the subcomponents, in which we take account of the separation energies to make the neutron holes by shifting the energy relatively.

B. Incident pion energy and elementary cross section

We choose the incident pion energies so as to satisfy the recoil free kinematics for the η meson production in nuclei. In this kinematics, η mesons can be created almost at rest in nuclei. The good advantage is that the formation spectra have less subcomponents due to the angular momentum selection rule for the η and neutron hole states [6, 9, 10, 18, 20], which makes the interpretation of the spectra much easier.

In Fig. 4, we plot the momentum transfer of the $A(\pi^+, p)(A-1)\eta$ reaction for the η energies $\omega = m_\eta$, $m_\eta - 50$ MeV with the proton angle being 0 and 15 degrees as functions of the incident pion momentum and pion kinetic energy. In the calculation of the momentum transfer, we take heavy mass limit for the initial and final nuclei. As Fig. 4 shows, depending on the η binding energy,

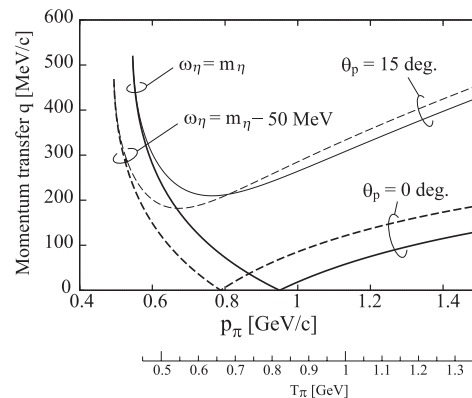


FIG. 4: Momentum transfers at η meson energies $\omega_\eta = m_\eta$ and $m_\eta - 50$ MeV as functions of the incident pion momentum p_π . θ_p denotes the emitted proton angle in the laboratory frame. The corresponding scale of the pion kinetic energy T_π is also shown.

this reaction with $\theta_p = 0$ has the magic momenta for the incident pion where the recoilless condition is satisfied. In this paper, we set the incident pion kinetic energies to be $T_\pi = 820$ MeV and $T_\pi = 650$ MeV to satisfy the recoilless condition at η threshold and $\omega_\eta = m_\eta - 50$ MeV, respectively. We stress here that these energies of the pion beam will be available at J-PARC facility [31].

We estimate the elementary cross section $\left(\frac{d\sigma}{d\Omega} \right)_{n(\pi^+, p)\eta}^{lab}$ using the experimental data of $\pi^- p \rightarrow n\eta$ measured by Crystal Ball collaboration [46]. We make use of isospin symmetry to obtain the cross section of $\pi^+ n \rightarrow p\eta$ from that of the Crystal Ball data. We calculate the η -mesic nucleus formation spectra with the incident pion energies of $T_\pi = 650, 820$ MeV in the laboratory frame. For these energies, we use the following values of the elementary cross section of $\pi^+ n \rightarrow p\eta$: $\left(\frac{d\sigma}{d\Omega} \right)_{n(\pi^+, p)\eta}^{lab} = 2.4$ mb/sr for $T_\pi = 650$ MeV and $\left(\frac{d\sigma}{d\Omega} \right)_{n(\pi^+, p)\eta}^{lab} = 0.64$ mb/sr for $T_\pi = 820$ MeV. The former value is read from the existent

experimental data, whereas the latter is taken from the partial-wave analysis (PAW) labeled by I375 [46], which is almost equivalent to the PAW FA02 [47].

C. Numerical results of the inclusive (π, N) spectra

In Fig. 5(1), we show the $^{12}\text{C}(\pi^+, p)^{11}\text{C} \otimes \eta$ cross sections for the formation of the η - ^{11}C system in the chiral doublet model with $C = 0.2$ (upper panel in Fig. 5(1)) and the chiral unitary model (lower panel in Fig. 5(1)). The incident pion kinetic energy T_π is 820 MeV corresponding to the recoilless at the η threshold. The horizontal axis indicates the excitation energy E_{ex} measured by the η production threshold E_0 . In the figure, we show the total spectra in solid line and the contributions from several subcomponents in dashed lines, separately. For the spectra of the subcomponents with the $(0s_{1/2})_n^{-1}$ neutron-hole state, which is an excited state of the daughter nucleus, the separation energy 18 MeV is taken into account. Thus the η meson production threshold appears at $E_{\text{ex}} - E_0 = 18$ MeV as indicated in Fig. 5 by the vertical dotted line. The Fig. 5(1) shows that the spectra are dominated by two contributions, $(0s_{1/2})_n^{-1} \otimes s_\eta$ and $(0p_{3/2})_n^{-1} \otimes p_\eta$, since the final states with the total spin $J \sim 0$ are largely enhanced under the recoilless kinematics.

Let us see the spectra around the threshold; -50 MeV $\lesssim E_{\text{ex}} - E_0 \lesssim 50$ MeV. The spectra in this energy region were already shown in the case of the $(d, ^3\text{He})$ and (γ, p) reactions in Refs. [9, 10, 18]. The present work confirms that the spectrum shape are very similar with the previous calculations, showing that the structure of the formation spectra is not sensitive to the reaction mechanism. As already discussed in detail in Refs. [9, 10, 18], the spectra obtained also in the (π^+, p) reaction around the η production threshold show that the repulsive nature of the optical potential in the chiral doublet model shifts the spectra into the higher energy region, whereas the spectra obtained in the chiral unitary model is shifted into the lower energy region as a result of its attractive potential.

Even with the distortion effects to the incident pion, we find that the difference of expected spectra in the (π^+, p) reaction between two approaches for N^* seems to be visible as the case with the (γ, p) reaction where the incident γ has no distortion effects.

In the case with the chiral doublet model, we can see the cusp structure in the $(0s_{1/2})_n^{-1} \otimes s_\eta$ subcomponent at $E_{\text{ex}} - E_0 = 18$ MeV corresponding to the η threshold for $(0s_{1/2})_n^{-1}$ hole states. This is so-called s -wave resonance which is found in the case with weak attraction. In this case with the chiral doublet model, the surface attractive pocket in the optical potential at the threshold plays the role of the weak attraction. In other words, we might be able to know the evidence of the curious shape of the optical potential in the doublet model from the spectral broadening into the higher energy region (associated with

the repulsion) together with the cusp structure at the threshold (associated with the weak attraction), if we could observe it. However, we should mention here that the s -hole state, corresponding to the excited state of the daughter nucleus, has natural width which is not taken into account in the present calculations. By considering the width of the s -hole state, the cusp structure could be smeared out from the spectrum.

Next, let us discuss the bound state structures. As reported in Refs. [10, 18], in chiral unitary model, we can see the bound state peak in the subcomponent $(0s_{1/2})_n^{-1} \otimes s_\eta$ around $E_{\text{ex}} - E_0 \sim 10 - 15$ MeV ($\omega_\eta - m_\eta \sim -10 - -5$ MeV) as indicated in the lower panel of Fig. 5(1). The existence of the bound state in the unitary model is predicted in Ref. [17]. As seen in the figure, however, it is impossible to observe the signals of the bound state, because there is large contribution from the $(0p_{2/3})_n^{-1} \otimes p_\eta$ subcomponent in the same energy and it masks the bound state peak in the $(0s_{1/2})_n^{-1} \otimes s_\eta$ component.

For the bound states in the case of the chiral doublet model, as reported in Ref. [20], there are some bound states obtained as solutions in the complex energy plane of the Klein-Gordon equation with the optical potential (5) in the chiral doublet model with $C = 0.2^1$. For η with $\ell_\eta = 0$, the bound states were found with the eigenenergies (B.E., Γ) = (91.3, 26.3) MeV for $0s$ and (75.1, 33.0) MeV for $1s$ [20]. In Fig. 5 we can see that the $0s$ bound state appears in the spectrum as a bump around $E_{\text{ex}} - E_0 \sim -70 - -80$ MeV. These deep bound states correspond to the lower mode mentioned in Sec. II in the chiral doublet model ($C = 0.2$). However, the strength of the bump in the spectrum is too small to be observed in experiments. The η bound states with $\ell_\eta = 1$ were also obtained at (79.3, 31.1) MeV for $0p$ and (72.1, 34.2) MeV for $1p$. The corresponding peak structure to the $0p$ bound state is not seen in the spectrum again due to the small strength. In the recoilless kinematics, the $1s$ and $1p$ bound states should give much less contributions in the spectrum, since there are no $1s$ - and $1p$ -hole states in the daughter nucleus for the carbon target case.

Much more prominent structure is seen in the quasi-free region $E_{\text{ex}} - E_0 > 0$ in the case of the chiral doublet model. As also discussed in detail in Ref. [20], we see considerably large bump structure around $E_{\text{ex}} - E_0 \sim 60$ MeV as shown in Fig. 5(1)(upper panel). This peak comes from the N^* -hole mode coupled to the η meson in the medium, namely the upper mode shown in Fig. 1(b). As discussed in Sec. II, the upper mode in the chiral doublet model is enhanced as a consequence of the level crossing associated with the reduction of the N - N^* mass gap in nuclear matter stemming from the partial restora-

¹ In Ref. [9], we did not search bound states with the chiral doublet potential $C = 0.2$ in energies $\omega - m_\eta \lesssim -50$ MeV, because such deep energies were out of scope of investigation in Ref. [9].

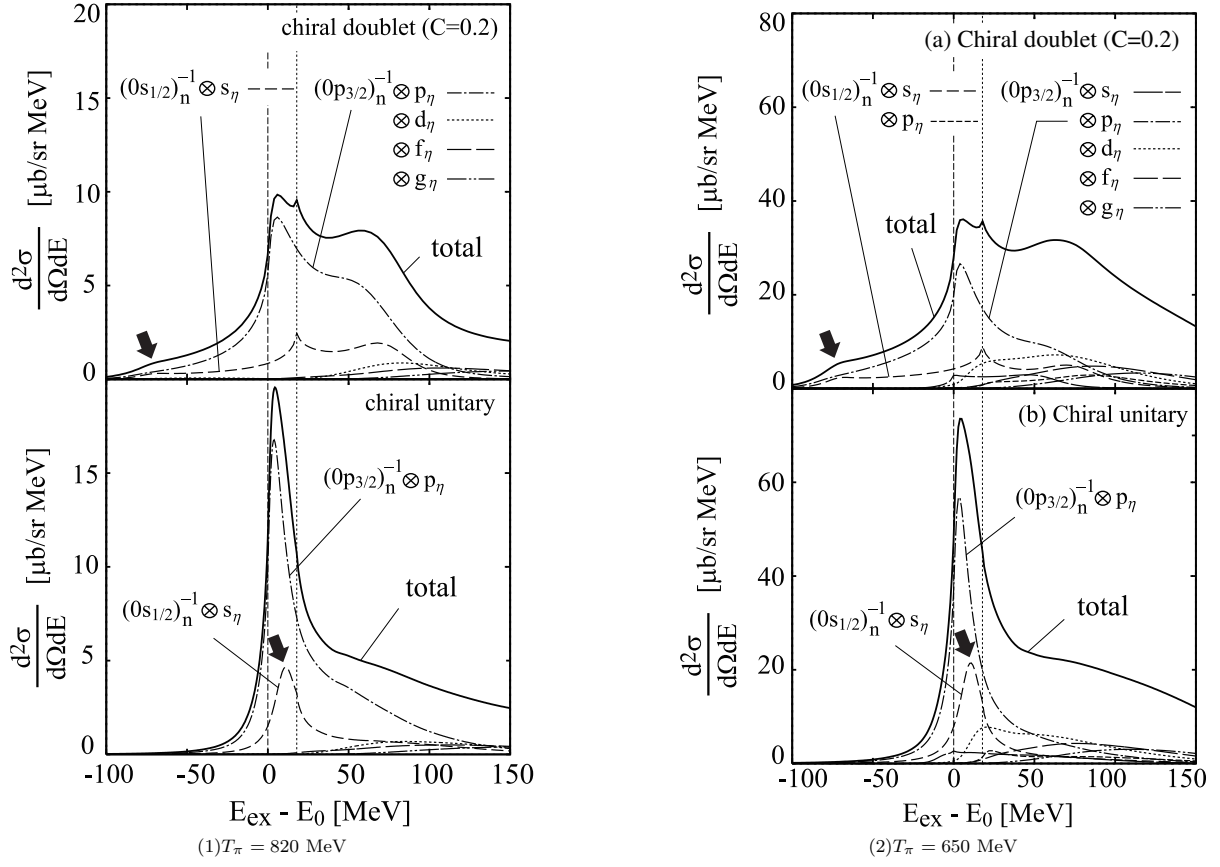


FIG. 5: Calculated spectra of $^{12}\text{C}(\pi^+, p)^{11}\text{C} \otimes \eta$ reaction at (1) $T_\pi = 820$ MeV and (2) $T_\pi = 650$ MeV and the proton angle $\theta_p = 0^\circ$ as functions of the excited energy E_{ex} . E_0 is the η production threshold. The η -nucleus interaction is calculated by using the chiral doublet model with $C = 0.2$ (upper panels) and the chiral unitary model (lower panels). The thick solid lines show the total spectra and dashed lines represent dominant subcomponents as indicated in the figures. The neutron-hole states are indicated as $(n\ell_j)_n^{-1}$ and the η states as ℓ_η . Solid arrow indicates the peak corresponding to the bound state in each model.

tion of the chiral symmetry. On the other hand, in the case of the chiral unitary approach, we see smooth slope in the quasi-free region. Hence, the enhancement in the quasi-free region could be a signal for the reduction of the N - N^* mass gap in nuclear medium, which supports the scenario of partial restoration of chiral symmetry in nuclear medium.

Finally, we mention the incident pion energy dependence of the spectra. In Fig. 5(2), we show the spectra with $T_\pi = 650$ MeV corresponding to the recoilless at $\omega_\eta - m_\eta \sim -50$ MeV. By setting the recoilless condition here, we have expected some enhancement of the deep bound state in the chiral doublet model. However, although small enhancement of the bound state can be seen, its effect is not large enough to make this bump clearly observed.

In $T_\pi = 650$ MeV case, we find that the magnitude of the cross section is four times larger than that of $T_\pi = 820$ MeV, because of the larger elementary cross section. We also find that, due to the relatively large momentum transfer (~ 100 MeV/c) at $T_\pi = 650$ MeV,

many subcomponents give finite contributions at quasi-free region, while in the $T_\pi = 820$ MeV case only two subcomponent $(0p_{3/2})_n^{-1} \otimes p_\eta$ and $(0s_{1/2})_n^{-1} \otimes s_\eta$ at almost all energy region shown there.

D. Spectra for πN coincident observation

In inclusive measurements, it may be hard to separate signals out of large backgrounds. It was argued for the previous (π^+, p) experiments in finite momentum transfer in Refs. [11, 23] that possible backgrounds could come from quasi-free knockout, multiple pion and proton scattering, and pion absorption and that the signal-noise ratio was estimated to be 1/10. It would be also expected in the present setup for the (π^+, p) reaction that the background can be as large as the previous experiment. To subtract such large background, it is useful to take some coincidence measurements accompanying the η meson production in nuclei, for example simultaneous observation of $N\pi$ pair coming from N^* decay in a nu-

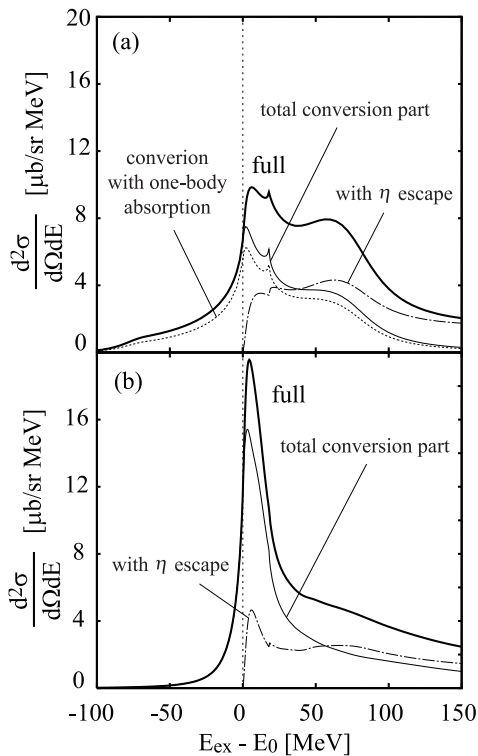


FIG. 6: Decomposition of the full spectra into the conversion parts and the escape part which are defined in the text. The reaction and energy are $^{12}\text{C}(\pi^+, p)^{11}\text{C} \otimes \eta$ and $T_\pi = 650$ MeV in (a) with the chiral doublet model and (b) the chiral unitary model. The full spectra are shown by the thick solid line and the conversion parts, which includes both of decay channels of $N^* \rightarrow N\pi$ and $N^*N \rightarrow NN\pi$, is shown by the thin solid line. The dashed line denotes the spectrum including only the $N^* \rightarrow N\pi$ conversion part, and the dot-dashed line denotes the escape part.

cleus [28, 32].

In the Green's function method [45], one can separately calculate each contribution to the spectrum coming from the different η absorption process. Along to the formalism in Ref. [45], we rewrite equivalently the imaginary part of the Green's function of η as

$$\text{Im}G = (1 + G^\dagger V_\eta^\dagger) \text{Im}G_0 (1 + V_\eta G) + G^\dagger \text{Im}V_\eta G \quad (12)$$

where G and G_0 denote the full and free Green's functions for η and V_η is the η optical potential. The first term of the right-hand-side of Eq. (12) represents the contributions from the escape of η from daughter nuclei and the second term describes the conversion process caused by the η absorption into the nuclei. Thus, calculating only the conversion part, we can show spectra associated with decays (or absorptions) of η mesons in nuclei, which can be obtained by observing emitted particles.

In the chiral doublet model, we take into account two decay channels of N^* in nuclear medium as mentioned in Sec. III; $N^* \rightarrow N\pi$ and $N^*N \rightarrow NN\pi$. These contri-

butions are expressed in the conversion part. Therefore, we can separate the spectra further into two terms by describing the conversion part as

$$\text{Im}V_\eta = \text{Im}V_\eta(N^* \rightarrow N\pi) + \text{Im}V_\eta(N^*N \rightarrow NN\pi). \quad (13)$$

As shown in Fig. 6(a), we decompose the total spectra shown in Fig. 5(1)(upper panel) into three parts; the contribution from the η -escape process, the conversion part of the $N^* \rightarrow N\pi$ and that of $N^*N \rightarrow NN\pi$ processes. The expected spectra with the coincidence of the $N\pi$ pair from N^* is indicated by the dotted line in the figure. The thin solid line in Fig. 6(a) includes both of the one-body and two-body absorption of N^* in the chiral doublet model. It is found that the $N^*N \rightarrow NN\pi$ contribution is much smaller than that of $N^* \rightarrow N\pi$. We also find that, in the doublet model case, the strength of the peak structure in the quasi-free region corresponding to the N^* -hole mode is reduced to be about half by taking the coincidence of $N\pi$ pair from N^* .

In Fig. 6(b), we plot the same figure for the chiral unitary model as Fig. 6(a). We only show the total conversion part, since decomposition of the η self-energy into different absorption processes was not done in the chiral unitary model. We expect that the difference between two approaches with and without the N^* mass reduction is still large even we take the coincidence of the N^* decay. In these estimation we do not take into account any final state interaction for emitted particles from N^* decay in a nucleus. These contributions could be important for further qualitative discussions.

For the background estimation in experiments, it would be useful to observe the (π^-, p) process in the same setup as the (π^+, p) . In the (π^-, p) process η mesons cannot be created due to isospin symmetry, and it is expected that the formation spectra have no structure at the η meson threshold. This means that all the contributions are regarded as “background”.

V. ADDITIONAL DISCUSSIONS ON EXPERIMENTAL FEASIBILITY

A. Comparison with the (π^+, p) reaction measured at Brookhaven

The (π^+, p) reaction experiment for the formation of the η -mesic nuclei has been already performed at Brookhaven in 1988 [23]. The experiment have been done at a finite proton angle $\theta_p = 15^\circ$ in the laboratory frame, based on the theoretical suggestion [11] to observe narrow peaks. The recoilless condition cannot be satisfied for finite angle proton emissions. In the case of $\theta_p = 15^\circ$, the momentum transfer is larger than 200 MeV/c in any incident pion momentum as shown in Fig. 4. Therefore, the expected spectra will be completely different from that of the forward angle.

We calculate the (π^+, p) spectra with the proton angle $\theta_p = 15^\circ$ and the incident pion energy $T_\pi = 673$ MeV

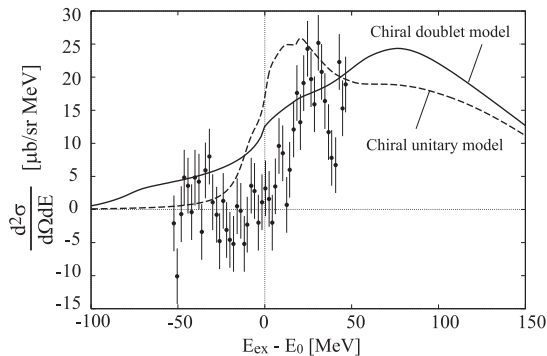


FIG. 7: Comparison of the calculated total spectra with the signal part of the experimental data on the carbon target case reported in Ref. [23] after the background subtraction shown in the same reference. The solid line indicates the total spectrum with the chiral doublet model ($C = 0.2$) and the dashed line is that of the chiral unitary model, calculated at the same condition with the data. In the theoretical calculations, the angular momentum of η is taken into account up to $\ell_\eta = 6$.

($p_\pi = 800$ MeV/c) in the same theoretical procedure as in the previous section, in order to compare the theoretical calculations with the experimental data obtained at Brookhaven. The comparison for the carbon target case is shown in Fig. 7. The data are taken from the second figure of Fig. 1 in Ref. [23] after subtraction of background estimated in the paper. They showed an experimental error bar only for one experimental point. We assume that the single error bar is a typical error for all the point and put the same error bar to all the point. We find in Fig. 7 that both models provide the consistent results with the experimental data. This means that the experiment with the finite proton angle in Ref. [23] is not sensitive to the in-medium properties of N^* [12, 13].

We show the details of the results calculated theoretically with finite proton angle in Fig. 8. We calculate the spectra by taking into account the η angular momenta up to $\ell_\eta = 6$. In the case of the finite proton angle, in contrast to the forward proton, many subcomponents have substantial contributions to the total spectra, especially higher angular momentum components $\ell_\eta \geq 1$, because the strong suppression for $J \neq 0$ configuration is not made any more. This makes it difficult to interpret the spectrum structure in terms of the properties of the η and N^* in nuclear medium.

In the spectrum calculated with the chiral unitary model, the lower panel of Fig. 8, two prominent peaks are seen around $E_{ex} - E_0 = -10$ MeV in the subcomponents $(0s_{1/2})_n^{-1} \otimes s_\eta$ and $(0p_{3/2})_n^{-1} \otimes s_\eta$ ². These are bound state signatures of the η meson with $\ell_\eta = 0$ in nuclei. In particular, it is interesting that the peak of

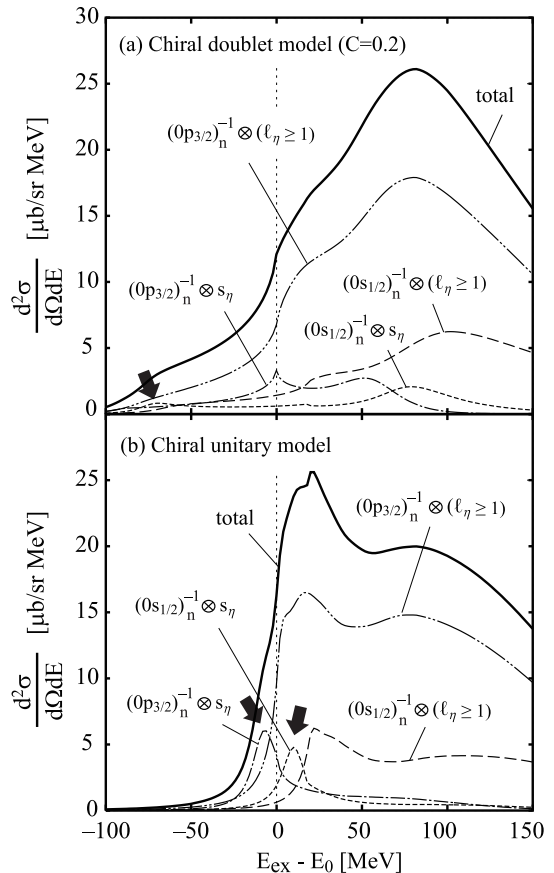


FIG. 8: Calculated spectra of $^{12}\text{C}(\pi^+, p)^{11}\text{C}\otimes\eta$ reaction at $T_\pi = 673$ MeV ($p_\pi = 800$ MeV/c) and the proton angle $\theta_p = 15^\circ$ as functions of the excited energy E_{ex} . E_0 is the η production threshold. The η -nucleus interaction is calculated by (a) the chiral doublet model with $C = 0.2$ and (b) the chiral unitary model. The thick solid lines show the total spectra and each dashed line represents the dominant subcomponent as indicated in the figures. The neutron-hole states are indicated as $(n\ell_j)_n^{-1}$ and the η states as ℓ_η . The angular momentum of η is taken into account up to $\ell_\eta = 6$. Solid arrows indicate the peaks corresponding to the bound states.

$(0p_{3/2})_n^{-1} \otimes s_\eta$ appears in bound region, where contamination from the quasi-free η contributions could be expected to be small. In fact, this observation was the original idea by Haider and Liu for the advantage of the finite proton angle experiment. As seen in the figure, however, this bound state peak is masked by the tail of the quasi-free contribution of $(0p_{3/2})_n^{-1} \otimes (\ell_\eta \geq 1)$ caused by virtual η absorption in the large imaginary potential. Thus, even if the chiral unitary model prediction of the bound state is correct, the bound state signal cannot be observed separately from the quasi-free contribution in the total spectrum. The same situation might have occurred in the Brookhaven experiment [23]. Therefore, the attempt to separate a shallow bound state from the quasi-free contribution by setting $\theta_p = 15^\circ$ seems not to work when the imaginary potential is large.

By all considerations mentioned above, we think that

² In the forward proton case, this subcomponent $(0p_{3/2})_n^{-1} \otimes s_\eta$ is strongly suppressed in the recoilless kinematics.

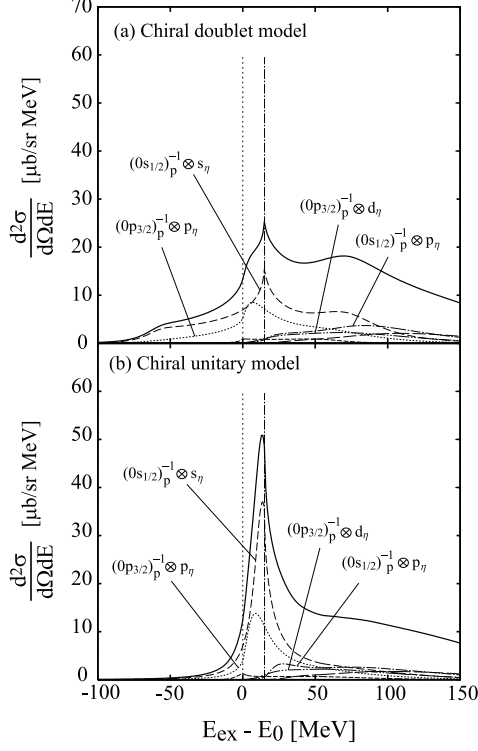


FIG. 9: Calculated spectra of ${}^7\text{Li}(\pi^-, n){}^6\text{He}\otimes\eta$ reaction at $T_\pi = 650$ MeV and the proton angle $\theta_p = 0^\circ$ as functions of the excited energy E_{ex} . E_0 is the η production threshold. The η -nucleus interaction is calculated by (a) the chiral doublet model with $C = 0.2$ and (b) the chiral unitary model. The thick solid lines show the total spectra and each dashed line represents the dominant subcomponent as indicated in the figures. Here, the proton-hole states are indicated as $(n\ell_j)_p^{-1}$ and the η states as ℓ_η .

it is better to set the final proton angle to be zero degree where the difference reflecting the distinct in-medium N^* properties expected to be larger. The energy range measured by the experiment [23] did not cover whole energies of the emitted proton where the interesting features, like the deep bound state and the bump structure in the quasi-free region caused by possible level crossing phenomena, take place.

B. (π^-, n) reaction with the ${}^7\text{Li}$ target

Here we show the formation spectra of the η -mesic nuclei in the (π^-, n) reaction with the ${}^7\text{Li}$ target. As shown in Figs. 5(1) and 5(2) for the carbon target, the total spectra were dominated by the p -wave components $(0p_{2/3})_n^{-1} \otimes p_\eta$ since the target nucleus ${}^{12}\text{C}$ has four neutrons in p -state while two in s -state. Then, the s -wave components are relatively small, which contain the interesting structure such as the bound states and/or the threshold cusp.

In Fig. 9, we show the spectra of ${}^7\text{Li}(\pi^-, n)$ reaction with the elementary process $\pi^- p \rightarrow n\eta$ (one proton picked-up). We see that the s -wave component now dominates the spectrum for each case (a) and (b), since ${}^7\text{Li}$ has a single proton in p -state. We can find a deep bound state peak in s_η state around $E_{\text{ex}} - E_0 \sim -60$ MeV in the chiral doublet model also in ${}^7\text{Li}$ target case while in the chiral unitary case we can see only the threshold peak structure. We consider that the experimental data with ${}^7\text{Li}$ target would be useful and be a complement to that of ${}^{12}\text{C}$.

C. Consideration of finite experimental resolution

We also estimate the effect of the finite experimental energy resolution on the spectra. For this purpose, we fold the calculated spectra with $T_\pi = 650$ MeV, which is shown in Fig. 5(2), as

$$\int f(E')g(E - E')dE', \quad (14)$$

where $f(E')$ represents the calculated spectra, and $g(E)$ expresses the effect of the finite energy resolution and is given in a gaussian form as

$$g(E - E') = \frac{1}{a\sqrt{\pi}} \exp \left[- \left(\frac{E - E'}{a} \right)^2 \right] \quad (15)$$

with $a = \Gamma_{\text{ex}}/2\sqrt{\ln 2}$. The experimental resolution (FWHM) is denoted by Γ_{ex} . In Fig. 10, we show the calculated result with several energy resolutions. We can observe the difference of two approaches with $\Gamma_{\text{ex}} \sim 20$ MeV, which are expected to be reached at J-PARC facility [31].

VI. CONCLUSION

We calculated the η -mesic nuclei formation spectra of (π, N) reactions with nuclear targets to discuss the experimental feasibility in forthcoming experiments. Emphasizing in-medium properties of the $N^*(1535)$ baryon resonance in the context of chiral symmetry, we discussed the structure of the η -mesic nuclei formation spectra. Especially, the reduction of N - N^* mass gap in the nuclear medium were investigated by two chiral models. In the chiral doublet model, $N^*(1535)$ is regarded as a chiral partner of nucleon and the mass gap is expected to be reduced in association with the partial restoration of the chiral symmetry in nuclear medium [9]. In the chiral unitary approach, $N^*(1535)$ is introduced as a resonance dynamically generated and described as a quasi-bound state of the Kaon and Hyperon, and reduction of the mass gap is expected to be small in nuclear matter [15, 16].

We showed the formation spectra of η -mesic nuclei by (π, N) reactions. We confirmed that the magnitude of

the cross section is large enough to be observed in experiments. We found that the (π, N) reactions were also appropriate to observe the interesting behaviors like deep bound states and the bump structure at the quasi-free region which can be understood by the concept of the level crossing phenomena caused by the partial restoration of the chiral symmetry [20]. We conclude that we can get new information on the in-medium N^* properties through the formation of the η -mesic nuclei by (π, N) reactions.

We also discussed expected background and ways of its reduction by the simultaneous observation of $N\pi$ pairs from the N^* decay in medium. We found that the difference between two treatments of in-medium N^* with and without the reduction of the N - N^* mass gap are not largely affected by the coincidence observation and there is some chance to make the observation clearer.

We believe that the present theoretical results are important to stimulate both theoretical and, especially, experimental activities to study the hadron properties in-medium and to obtain new information on the partial restoration of the chiral symmetry in nuclear medium.

Acknowledgement

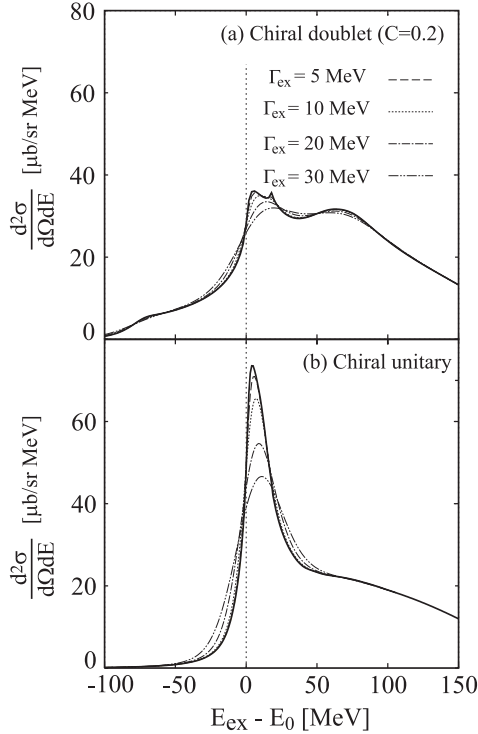


FIG. 10: Convolutions of the spectra of $^{12}\text{C}(\pi^+, p)^{11}\text{C} \otimes \eta$ reaction at $T_\pi = 650$ MeV and the proton angle $\theta_p = 0^\circ$. The thick solid lines indicate the spectra without convolution, and other lines are spectra taken convolutions with finite experimental resolution Γ_{ex} indicated in the figures.

We would like to express our thanks to E.E. Kolomeitsev for fruitful collaboration. We also thank K. Itahashi and H. Fujioka for the useful discussions from experimental side. One of the author (H. N.) is the Research Fellow of the Japan Society for the Promotion of Science (JSPS). This work is partially supported by the Grant for Scientific Research (No. 18-8661, 18042001, 20028004). A part of this work was done under Yukawa International Project for Quark-Hadron Science (YIPQS).

[1] For example; C.J. Batty, E. Friedman and A. Gal, Phys. Rept. **287**, 385 (1997); E. Friedman, A. Gal, Phys. Rept.

- [2] H. Toki, S. Hirenzaki, T. Yamazaki, Nucl. Phys. **A530**, 679 (1991); S. Hirenzaki, H. Toki, T. Yamazaki, Phys. Rev. **C44**, 2472 (1991).
- [3] H. Gilg *et al.*, Phys. Rev. C **62**, 025201 (2000); K. Itahashi, *et al.*, *ibid.* **62**, 025202 (2000).
- [4] H. Geissel *et al.*, Phys. Rev. Lett. **88**, 122301 (2002).
- [5] P. Kienle, and T. Yamazaki, Phys. Lett. B **514**, 1 (2001); H. Geissel, *et al.*, *ibid.* **549**, 64 (2002); K. Suzuki, *et al.*, Phys. Rev. Lett. **92**, 072302 (2004).
- [6] R.S. Hayano, S. Hirenzaki, A. Gillitzer, Eur. Phys. J. A **6**, 99 (1999).
- [7] K. Tsushima, D.H. Lu, A.W. Thomas, K. Saito, Phys. Lett. **B443**, 26 (1998); K. Tsushima, D.H. Lu, A.W. Thomas, Phys. Rev. **C59**, 1203 (1999).
- [8] S. Hirenzaki, H. Nagahiro, T. Hatsuda, T. Kunihiro, Nucl. Phys. **A710**, 131 (2002).
- [9] D. Jido, H. Nagahiro and S. Hirenzaki, Phys. Rev. **C66**, 045202 (2002); Nucl. Phys. **A721**, 665c(2003).
- [10] H. Nagahiro, D. Jido and S. Hirenzaki, Phys. Rev. **C68**, 035205 (2003).
- [11] Q. Haider and L. C. Liu, Phys. Lett. B **172** (1986) 257, L. C. Liu and Q. Haider, Phys. Rev. C **34** (1986) 1845.
- [12] M. Kohno and H. Tanabe, Phys. Lett. **B** 231(1989) 219-223.
- [13] M. Kohno and H. Tanabe, Nucl. Phys. A **519** (1990) 755.
- [14] H. C. Chiang, E. Oset and L. C. Liu, Phys. Rev. C **44** (1991) 738.
- [15] T. Waas and W. Weise, Nucl. Phys. A **625** (1997) 287.
- [16] T. Inoue and E. Oset, Nucl. Phys. A **710** (2002) 354.
- [17] C. Garcia-Recio, J. Nieves, T. Inoue and E. Oset, Phys. Lett. **B550**, 47 (2002).
- [18] H. Nagahiro, D. Jido and S. Hirenzaki, Nucl. Phys. A **761**, 92 (2005).
- [19] N. G. Kelkar, K. P. Khemchandani and B. K. Jain, J. Phys. G **32**, L19 (2006)
- [20] D. Jido, E. E. Kolomeitsev, H. Nagahiro and S. Hirenzaki, Nucl. Phys. A **811**, 158 (2008).
- [21] C. Y. Song, X. H. Zhong, L. Li and P. Z. Ning, Europhys. Lett. **81**, 42002 (2008)
- [22] J. Yamagata, H. Nagahiro and S. Hirenzaki, Phys. Rev. C **74** (2006) 014604 [arXiv:nucl-th/0602021].
- [23] R. E. Chrien *et al.*, Phys. Rev. Lett. **60** (1988) 2595.
- [24] J. Berger *et al.*, Phys. Rev. Lett. **61**, 919 (1988).
- [25] J. D. Johnson *et al.*, Phys. Rev. C **47**, 2571 (1993).
- [26] M. Pfeiffer *et al.*, Phys. Rev. Lett. **92**, 252001 (2004).
- [27] C. Hanhart, Phys. Rev. Lett. **94**, 049101 (2005) [arXiv:hep-ph/0408204].
- [28] G.A. Sokol and V.A. Tryasuchev, Sov. Phys. Lebedev Inst. Rep. 4, 23 (1991); G. A. Sokol, T. A. Aibergenov, A. V. Kravtsov, A. I. L'vov and L. N. Pavlyuchenko, Fizika B **8**, 85 (1999).
- [29] V. A. Baskov *et al.*, arXiv:nucl-ex/0306011.
- [30] M. K. Anikina *et al.*, arXiv:nucl-ex/0412036.
- [31] K. Itahashi and H. Fujioka, in private communication; K. Itahashi, H. Fujioka, S. Hirenzaki, D. Jido, and H. Nagahiro, Letter of Intent for J-PARC, "Spectroscopy of η mesic nuclei via ${}^7\text{Li}(\pi, n)$ reaction at recoilless kinematics" (2007).
- [32] V. Jha, et al., GEM Collaboration, Int. J. Mod. Phys. A **22**, 596 (2007) .
- [33] See the reviews, T. Hatsuda and T. Kunihiro. Phys. Rep. **247**, 221 (1994); G.E. Brown and M. Rho, *ibid.* **269**, 333 (1996).
- [34] D. Jido, T. Hatsuda and T. Kunihiro, Phys. Lett. B, in press.
- [35] C. DeTar and T. Kunihiro, Phys. Rev. D **39** (1989) 2805.
- [36] D. Jido, Y. Nemoto, M. Oka and A. Hosaka, Nucl. Phys. A **671** (2000) 471; Y. Nemoto, D. Jido, M. Oka and A. Hosaka, Phys. Rev. D **57** (1998) 4124.
- [37] D. Jido, M. Oka and A. Hosaka, Prog. Theor. Phys. **106** (2001) 873.
- [38] C. Amsler *et al.* [Particle Data Group], Phys. Lett. B **667**, 1 (2008).
- [39] T. Hatsuda, T. Kunihiro and H. Shimizu, Phys. Rev. Lett. **82** (1999) 2840.
- [40] $C = 0.2$ is consistent with the calculation of the chiral condensate done in H. c. Kim, D. Jido and M. Oka, Nucl. Phys. A **640** (1998) 77.
- [41] N. Kaiser, P. B. Siegel and W. Weise, Phys. Lett. B **362**, 23 (1995).
- [42] T. Inoue, E. Oset and M. J. Vicente Vacas, Phys. Rev. C **65**, 035204 (2002).
- [43] E. E. Kolomeitsev and M. F. M. Lutz, Phys. Lett. B **585**, 243 (2004).
- [44] T. Hyodo, D. Jido and A. Hosaka, Phys. Rev. C **78**, 025203 (2008); D. Jido, T. Hyodo and A. Hosaka, Mod. Phys. Lett. A **23**, 2389 (2008).
- [45] O. Morimatsu and K. Yazaki, Nucl. Phys. A **435** (1985) 727, O. Morimatsu and K. Yazaki, Nucl. Phys. A **483** (1988) 493.
- [46] S. Prakhov *et al.*, Phys. Rev. C **72** (2005) 015203.
- [47] R. A. Arndt, W. J. Briscoe, I. I. Strakovsky, R. L. Workman and M. M. Pavan, Phys. Rev. C **69**, 035213 (2004).